Research Paper
Computational Methods for Differential Equations
http://cmde.tabrizu.ac.ir
Vol. 14, No. 2, 2026, pp. 502-518
DOI:10.22034/cmde.2025.58316.2465

A mathematical and computational study of global stability in partially-ionized rotating plasma

Vishal Chandel[1,*], **Sunil**[1], **and Poonam Sharma**[2]

[1]Department of Mathematics & Scientific Computing, National Institute of Technology Hamirpur, Hamirpur, 177005, Himachal Pradesh, India.

[2]Department of Mathematics, Govt. College Jawalaji, Jawalamukhi, Kangra, 176031, Himachal Pradesh, India.

Abstract

A mathematical and computational study of the impact of rotation on the thermal convection of partially-ionized plasma has been explored using both linear and nonlinear analyses. The method of normal mode analysis has been used to study the linear analysis whereas, for nonlinear analysis, we have used the generalized energy method. For numerical analysis, we have employed the Galerkin method. It has been found that the Rayleigh number for nonlinear analysis is the same as stationary convection. Hence, we concluded that there is no sub-critical region and the system is globally stable. The effect of collision plays an important role in the energy decay analysis. It has also been observed that for stationary convection, the collisional frequency has no impact on stability, whereas rotation stabilizes the system. The effect of various parameters has also been discussed for oscillatory convection. The stability characteristics for different bounding surfaces are examined. For low rotation rates, partially ionized plasma confined between rigid–rigid boundaries is the most stable configuration; however, at high rotation rates, the free–free bounding surfaces yield the greatest stability.

Keywords. Thermal convection, rotation, compressible partially-ionized plasma.

2010 Mathematics Subject Classification. 76E06, 76E07, 82D10.

1. Introduction

In many areas of fluid dynamics, the theory of Bénard convection is considered a basic problem of uttermost importance. In 1900, Bénard demonstrated the onset of thermal convection in fluid [5]. In most circumstances, the expansion of fluid in the bottom portion is a result of the rising temperature of the fluid layer, which is heated from below, and hence becomes lighter as compared to the fluid in the upper layer. This system is potentially unstable due to the top-heavy arrangement. When the difference in temperature or the depth of layer is adequately large, fluid will tend to redistribute itself. In this redistribution, lighter fluid rises to the top and heavier fluid sinks to the bottom. This cycle of rising and sinking creates a continuous flow of the fluid, allowing heat to transfer from one place to another. This motion has a stationary cellular character, which is observed as a regular hexagonal pattern so long as proper precautions are taken when doing the experiment. Lord Rayleigh established the theoretical framework for a valid explanation of Bénard's experiment in 1916.

Bénard convection with rotation has been studied extensively, both experimentally and theoretically [5, 6, 10, 15]. The Coriolis effect causes the pattern of convection cells to alter as the system rotates. The rotation of the system and conservation of the fluid's angular momentum led to the Coriolis effect. The impact causes the fluid to travel in a spiral pattern, which can either strengthen or weaken the convection cells, depending on the direction of rotation. In many fields of engineering and geophysical fluid dynamics, such as the study of the Earth's mantle and the dynamics of ocean currents, it is crucial to understand the interaction between rotation and convection.

Received: 06 September 2023; Accepted: 10 April 2025.
∗ Corresponding author. Email: vcvishal1950chandel@gmail.com.

Partially-ionized plasma (PIP) is a state of matter made up of both charged and neutral particles. Molecular clouds, cometary tail, the solar atmosphere, the interstellar medium and many other astronomical environments all include partially-ionized plasma with varying degrees of ionization [13]. Numerous examples of interaction between neutral and ionized gas constituents in cosmic physics have been discussed by Alfvén [1]. The dynamics of plasma are significantly affected by the interaction of charged and neutral components. Fluid instabilities such as thermal, thermosolutal, Rayleigh-Taylor and Kelvin-Helmholtz have been demonstrated to be influenced by the effect of partial-ionization [13]. The properties of PIP can be quite complex and depend on various factors, such as temperature, pressure, and the composition of the plasma. It has been essential to understand and control these properties for many practical applications, such as energy production, weather forecasting of space and plasma medicine.

The physical significance of thermal convection in a rotating PIP has been observed in various laboratory and astrophysical plasmas. The Coriolis force due to the rotation of plasma affects the fluid flow and thermal convection processes. In astrophysics, for example, the rotation of stars can lead to the formation of convection cells in the PIP within the stars. The rotation can modify the size and shape of the cells, affecting the transport of energy and material within the stars. The resulting thermal and magnetic structures can have important implications for the evolution of the stars and the production of heavy elements.

Previously, the linear study of the effect of collision and the effect of rotation for free-free bounding surfaces has been studied by Pensia, Shrivastava and Patidar [9], Sharma and Sharma [10], Sharma and Sunil [12] and Sunil and Sharma [18] and references therein. More recent studies by Chandel and Sunil [3] and Chandel et al. [4] investigated the effects of rotation and magnetic fields on the onset of thermal convection in PIP, considering different boundary configurations. Their findings, based on the single-term Galerkin method for numerical analysis, indicated consistent stability results across both linear and nonlinear analyses for various boundary conditions. Nonlinear and linear analyses with different boundary conditions have not been explored in any of the aforementioned studies. Nonlinear analysis provides a more accurate representation of the complex behaviour of the system, including the effect of nonlinear interactions between different physical processes. Also, this theory predicts sufficient conditions for stability. On the other hand, a linear analysis yields sufficient criteria for the instability of the system. The different boundary analyses are a crucial part of our study, as different boundary conditions impose different conditions on PIP, such as rigid-rigid boundaries imposing a no-slip boundary condition.

Keeping in view the importance of current investigation in engineering applications, including a variety of astronomical phenomena, our works deal with the linear and nonlinear analyses of a rotating compressible PIP, confined in different combinations of bounding surfaces. Linear analysis has been studied by the normal mode analysis method [5, 16], whereas a generalized energy method [6, 15] has been used for nonlinear analysis. For numerical computation, the Galerkin method has been employed [2, 7, 17]. Also, the influence of rotation, collisional frequency and compressibility on stationary and oscillatory convection for all three mentioned bounding surfaces has been explored in this work. To the best of our knowledge, linear and nonlinear analyses by including the effect of rotation and compressibility for different bounding surfaces have not been explored before, so this study will be of great practical importance in the field of plasma dynamics.

2. Formulation of physical problem and perturbed equations

We consider a horizontal infinite layer of thickness d of compressible partially-ionized plasma, having density ρ, which is permeated with the neutral components of density ρ_d. This layer is acted on by a gravitational force in negative z-direction i.e., $\mathbf{g} = (0, 0, -g)$ and a uniform vertical rotation $\mathbf{\Omega} = (0, 0, \Omega)$. This infinite horizontal layer of composite plasma is heated from below and a uniform temperature gradient $\beta \left(= \left|\frac{dT}{dz}\right|\right)$ is maintained. Figure 1 represents the geometrical configuration of the physical system.

Here, we make the assumption that the partially-ionized plasma obeys the continuum hypothesis and behaves like a continuum fluid. Moreover, the effects of rotation, pressure and gravity on the neutral components of this partially-ionized plasma are negligibly small, so they can be ignored.

The equations governing the flow of rotating compressible partially-ionized plasma [8–10, 18] are

$$\frac{\partial \rho}{\partial t} + (\mathbf{q} \cdot \nabla)\, \rho + \rho \nabla \cdot \mathbf{q} = 0, \tag{2.1}$$

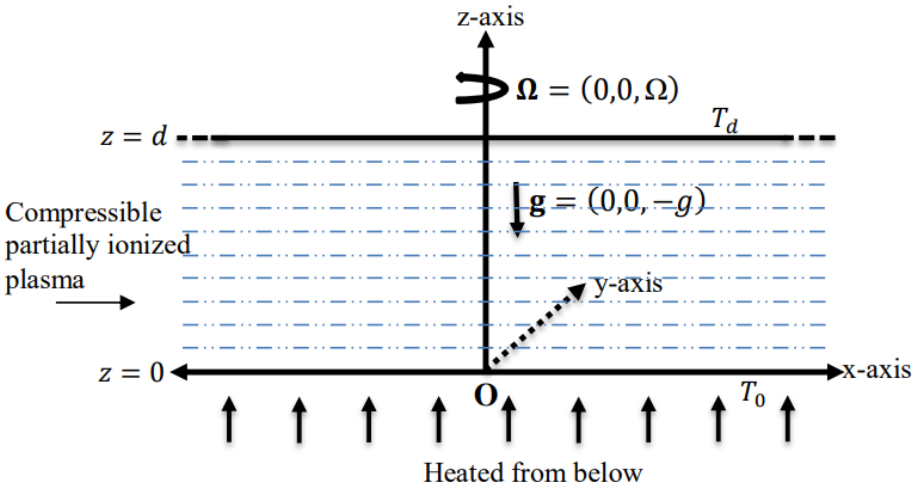

FIGURE 1. Geometrical configuration of the physical system.

$$\frac{\partial \mathbf{q}}{\partial t}+(\mathbf{q}\cdot\nabla)\mathbf{q}=-\frac{1}{\rho_m}\nabla p+\mathbf{g}\frac{\rho}{\rho_m}+\frac{\mu}{\rho_m}\nabla^2\mathbf{q}+\frac{\rho_d\nu_c}{\rho_m}(\mathbf{q}_d-\mathbf{q})+2(\mathbf{q}\times\mathbf{\Omega}), \tag{2.2}$$

$$\frac{\partial T}{\partial t}+(\mathbf{q}\cdot\nabla)T+p(\nabla\cdot\mathbf{q})=\kappa\nabla^2 T, \tag{2.3}$$

$$\rho=\rho_m\left[1-\alpha(T-T_m)+K_m(p-p_m)\right]. \tag{2.4}$$

In writing Eq. (2.2), the use of the Boussinesq approximation has been made.

Equation of motion for neutral components will consist of an opposite and equal term to that in Eq. (2.2) for ionized components and so it can be written as

$$\frac{\partial \mathbf{q}_d}{\partial t}+(\mathbf{q}_d\cdot\nabla)\mathbf{q}_d=-\nu_c(\mathbf{q}_d-\mathbf{q}). \tag{2.5}$$

Here, $\mathbf{q}$, $\mathbf{q}_d$, t, ρ_0, ρ_m, ρ_d, p, μ, ν_c, ν, c_p, κ, T, T_0, T_m, T_d and α denote the velocity of ionized components of PIP, velocity of the neutral components of PIP, time, density at $z=0$, constant space average of density, density of the neutral components of PIP, pressure, coefficient of viscosity, collisional frequency among the composite medium components, kinematic viscosity, specific heat at constant pressure, thermal diffusivity, temperature, temperature at $z=0$, temperature at which $\rho=\rho_m$, temperature at $z=d$ and coefficient of thermal expansion, respectively.

The contributing terms due to the presence of rotation: (a) $-\frac{1}{2}\text{grad}\left(|\mathbf{\Omega}\times\mathbf{r}|^2\right)$ (i.e., Centrifugal force) and (b) $2(\mathbf{\Omega}\times\mathbf{q})$ (i.e., Coriolis acceleration) [5]. Here, the centrifugal force combines with the pressure term in Eq. (2.2) to become the reduced pressure, defined as $p=p_f-\frac{\rho_0}{2}|\mathbf{\Omega}\times\mathbf{r}|^2$, where p_f stands for fluid pressure. On the other hand, the effect of Coriolis acceleration has been studied by examining the effect of rotation.

Here, we assume the steady basic state [11], which is given by $\mathbf{q}=\mathbf{q}_b=\mathbf{0}$, $\rho=\rho_b(z)$, $p=p_b(z)$, $T=T_b(z)$ and $\mathbf{q}_d=\mathbf{q}_{d_b}=\mathbf{0}$, where we have

$$\begin{aligned}
&p_b(z)=p_m-g\int_0^z(\rho_m+\rho_0)\,dz,\\
&\rho_b(z)=\rho_m\left[1-\alpha(T-T_m)+K_m(p-p_m)\right],\\
&T_b(z)=-\beta z+T_0,\\
&\alpha=-\left(\frac{1}{\rho}\frac{\partial\rho}{\partial T}\right)_m,\quad K_m=-\left(\frac{1}{\rho}\frac{\partial\rho}{\partial p}\right)_m,
\end{aligned} \tag{2.6}$$

where the basic state is represented by the subscript 'b'.

The state variables: pressure, temperature or density can be stated in the form of

$$X\left(x,y,z,t\right)=X'(x,y,z,t)+X_0(z)+X_m,$$

where X' is the fluctuation resulting from the motion, X_0 is the change when there is no motion and X_m is the constant space average of X [11, 14].

Consider $\mathbf{q}'=(u,v,w)$, θ, $\delta\rho$, p' and $\mathbf{q}_d^{'}=(\ell,r,s)$ be the small perturbations in velocity of ionized component, temperature, density, pressure and velocity of neutral component of partially-ionized plasma, respectively. The change in the density is given by $\delta\rho=-\rho_m\alpha\theta$, which is due to the perturbation in temperature. Then the appropriate equations for perturbation, under the approximations of Spiegel and Veronis [14], are

$$\nabla\cdot\mathbf{q}'=0, \tag{2.7}$$

$$\frac{\partial\mathbf{q}'}{\partial t}+(\mathbf{q}'\cdot\nabla)\mathbf{q}'=-\frac{1}{\rho_m}\nabla p'+\alpha\theta g\hat{\mathbf{k}}+\nu\nabla^2\mathbf{q}'+\frac{\rho_d\nu_c}{\rho_m}\left(\mathbf{q}_d^{'}-\mathbf{q}'\right)+2\left(\mathbf{q}'\times\mathbf{\Omega}\right), \tag{2.8}$$

$$\frac{\partial\theta}{\partial t}+\left(\mathbf{q}'\cdot\nabla\right)\theta=\kappa\nabla^2\theta+\left(\beta-\frac{g}{c_p}\right)w, \tag{2.9}$$

$$\frac{\partial\mathbf{q}_d^{'}}{\partial t}+(\mathbf{q}_d^{'}\cdot\nabla)\mathbf{q}_d^{'}=-\nu_c\left(\mathbf{q}_d^{'}-\mathbf{q}'\right). \tag{2.10}$$

The boundary conditions (BCs) are

$$\mathbf{q}'=\mathbf{0},\ \mathbf{q}_d^{'}=\mathbf{0},\ \theta=0\text{ at }z=0,d,$$

and plane tiling periodicity is satisfied by $\mathbf{q}'$, $\mathbf{q}_d^{'}$, θ.

3. Stability analysis (nonlinear)

To investigate the stability using the energy method, the governing Eqs. (2.7)–(2.10) in non-dimensional form by using the following non-dimensional quantities and non-dimensional parameters

$$t=\tfrac{d^2}{\nu}t^*,\ \mathbf{q}'=\tfrac{\nu}{d}\mathbf{q}^*,\ \mathbf{q}_d^{'}=\tfrac{\nu}{d}\mathbf{q}_d^*,\ z=z^*d,\ \theta=\tfrac{\beta dPr}{R^{1/2}}\theta^*,\ p'=\tfrac{\rho_0\nu^2}{d^2}p^*,$$
$$R=\tfrac{g\alpha\beta d^4}{\nu\kappa},\ F=\tfrac{\rho_d}{\rho_0},\ L=\tfrac{\nu_c d^2}{\nu},\ Pr=\tfrac{\nu}{\kappa},\ T_A=\left(\tfrac{2\Omega d^2}{\nu}\right)^2\text{ and }G=\tfrac{c_p\beta}{g}.$$

Here, R, L, Pr, T_A, and G denote Rayleigh number, the parameter to measure the effect of collisional frequency, Prandtl number, Taylor number and compressibility parameter, respectively. The non-dimensional form (dropping asterisk) of the perturbation Eqs. (2.7)–(2.10) are given as

$$\nabla\cdot\mathbf{q}=0, \tag{3.1}$$

$$\frac{\partial\mathbf{q}}{\partial t}+(\mathbf{q}\cdot\nabla)\mathbf{q}=-\nabla p+R^{1/2}\theta\hat{\mathbf{k}}+\nabla^2\mathbf{q}+FL\left(\mathbf{q}_d-\mathbf{q}\right)+T_A^{1/2}\left(\mathbf{q}\times\hat{\mathbf{k}}\right), \tag{3.2}$$

$$Pr\left[\frac{\partial\theta}{\partial t}+\left(\mathbf{q}\cdot\nabla\right)\theta\right]=\nabla^2\theta+\left(1-\frac{1}{G}\right)R^{1/2}w, \tag{3.3}$$

$$\frac{\partial\mathbf{q}_d}{\partial t}+(\mathbf{q}_d\cdot\nabla)\mathbf{q}_d=-L\left(\mathbf{q}_d-\mathbf{q}\right). \tag{3.4}$$

Now, let us observe the effect of the collisional frequency of neutral components on the decay of energy. Since the convective term of the equation of momentum of neutral components is free from collisional frequency, we ignore this term and focus on finding the value of velocity of neutral components from Eq. (3.4), by using the normal mode analysis technique, where we are looking for a solution whose time dependence is of the form

$$f(z).\exp\left\{\iota\left(k_xx+k_yy\right)+nt\right\},$$

where k_x and k_y $\left(a^2 = k_x^2 + k_y^2\right)$ are horizontal wave numbers and n is the frequency of the harmonic disturbances [10]. Letting $n \equiv \frac{\partial}{\partial t}$, we have from Eq. (3.4),

$$\mathbf{q}_d = \frac{L}{n+L}\mathbf{q}. \tag{3.5}$$

Using Eqs. (3.5) and (3.2) becomes

$$\left[1 + FL(n+L)^{-1}\right] n\mathbf{q} + (\mathbf{q}\cdot\nabla)\,\mathbf{q} = -\nabla p + R^{1/2}\theta\hat{\mathbf{k}} + \nabla^2\mathbf{q} + T_A^{1/2}\left(\mathbf{q}\times\hat{\mathbf{k}}\right). \tag{3.6}$$

Now, applying the operator $\hat{\mathbf{k}}\cdot$ curl and $\hat{\mathbf{k}}\cdot$ curlcurl on Eq. (3.6), we have

$$\left[1 + FL(n+L)^{-1}\right] n\zeta + \hat{\mathbf{k}}\cdot\operatorname{curl}\left[(\mathbf{q}\cdot\nabla)\,\mathbf{q}\right] = \nabla^2\zeta + T_A^{1/2} w_z, \tag{3.7}$$

$$\left[1 + FL(n+L)^{-1}\right] n\nabla^2 w - \hat{\mathbf{k}}\cdot\operatorname{curlcurl}\left[(\mathbf{q}\cdot\nabla)\,\mathbf{q}\right] = R^{1/2}\nabla_1^2\theta + \nabla^4 w - T_A^{1/2}\zeta_z. \tag{3.8}$$

Also, from Eq. (3.3), we get

$$Pr\left[\frac{\partial\theta_z}{\partial t} + (\mathbf{q}_z\cdot\nabla)\,\theta + (\mathbf{q}\cdot\nabla)\,\theta_z\right] = \nabla^2\theta_z + \left(1 - \frac{1}{G}\right) R^{1/2} w_z. \tag{3.9}$$

Multiplying Eq. (3.7) by ζ, Eq. (3.8) by w, and Eq. (3.9) by θ_z and using integration over V, we get

$$\frac{1}{2}\left[1 + \frac{FL}{n+L}\right]\frac{d}{dt}\|\zeta\|^2 = -T_A^{1/2}\langle w\zeta_z\rangle - \|\nabla\zeta\|^2 - \langle\zeta\hat{\mathbf{k}}\cdot\operatorname{curl}\left[(\mathbf{q}\cdot\nabla)\,\mathbf{q}\right]\rangle, \tag{3.10}$$

$$\frac{1}{2}\left[1 + \frac{FL}{n+L}\right]\frac{d}{dt}\|\nabla w\|^2 = R^{1/2}\langle\nabla_1 w\nabla_1\theta\rangle - \left\|\nabla^2 w\right\|^2 - \langle w\hat{\mathbf{k}}\cdot\operatorname{curlcurl}\left[(\mathbf{q}\cdot\nabla)\,\mathbf{q}\right]\rangle + T_A^{1/2}\langle w\zeta_z\rangle, \tag{3.11}$$

$$\frac{Pr}{2}\frac{d}{dt}\|\theta_z\|^2 = \left(\frac{G-1}{G}\right) R^{1/2}\langle w_z\theta_z\rangle - \|\nabla\theta_z\|^2 + Pr\langle\theta_{zz}\mathbf{q}\cdot\nabla\theta\rangle, \tag{3.12}$$

where $\langle\cdot\rangle$ denotes the integration over V; $\|\cdot\|$ denotes the $L^2(V)$ norm; and V denotes typical periodicity cell.

Now an L^2 energy, $E(t)$, is constructed to study the nonlinear stability, from Eqs. (3.10)–(3.12), the evolution of energy is as follows

$$\frac{dE}{dt} = I_0 - D_0 + N_0. \tag{3.13}$$

Here,

$$E = \frac{\lambda_1}{2}\left[1 + \frac{FL}{n+L}\right]\|\nabla w\|^2 - \frac{\lambda_2}{2}\left[1 + \frac{FL}{n+L}\right]\|\zeta\|^2 + \frac{Pr}{2}\|\theta_z\|^2, \tag{3.14}$$

$$I_0 = \left(\frac{G-1}{G}\right) R^{1/2}\langle w_z\theta_z\rangle + \lambda_1 R^{1/2}\langle\nabla_1 w\nabla_1\theta\rangle + T_A^{1/2}(\lambda_1+\lambda_2)\langle w\zeta_z\rangle, \tag{3.15}$$

$$D_0 = \lambda_1\left\|\nabla^2 w\right\|^2 - \lambda_2\|\nabla\zeta\|^2 + \|\nabla\theta_z\|^2, \tag{3.16}$$

$$N_0 = Pr\langle\theta_{zz}\mathbf{q}\cdot\nabla\theta\rangle - \lambda_1\langle w\hat{\mathbf{k}}\cdot\operatorname{curlcurl}\left[(\mathbf{q}\cdot\nabla)\,\mathbf{q}\right]\rangle + \lambda_2\langle\zeta\hat{\mathbf{k}}\cdot\operatorname{curl}\left[(\mathbf{q}\cdot\nabla)\,\mathbf{q}\right]\rangle, \tag{3.17}$$

with λ_1 and λ_2 being two positive coupling parameters.

Here, energy is consumed due to rotation, as indicated by the negative sign with the term $\frac{\lambda_2}{2}\|\zeta\|^2$ in the energy equation (3.14).

Now, defining

$$m = \max_{H} \frac{I_0}{D_0}, \tag{3.18}$$

where H is admissible solution space.

Then, we require $m < 1$, so that

$$\frac{dE}{dt} \leq -a_o D_0 + N_0, \tag{3.19}$$

where $a_o = 1 - m\,(> 0)$.

3.1. **Construction of generalized energy.** Generalized energy functional is introduced to study the (conditional) nonlinear stability and to dominate the nonlinear terms, which is given as

$$E_g\,(t) = E\,(t) + b_o E_1\,(t)\,, \tag{3.20}$$

and the complementary energy $E_1(t)$ is given by

$$E_1\,(t) = \frac{1}{2}\left[1 + \frac{FL}{n+L}\right]\|\nabla \mathbf{q}\|^2 + \frac{Pr}{2}\|\nabla\theta\|^2, \tag{3.21}$$

where b_o in Eq. (3.20) is a positive coupling parameter.

$$\frac{dE_g}{dt} \leq -a_0 D_0 + N_0 + b_0 I_1 - b_o D_1 + b_0 N_1, \tag{3.22}$$

is the evolution of $E_g\,(t)$.

Here,

$$I_1 = \left(\frac{2G-1}{G}\right) R^{1/2}\ \langle \nabla w \cdot \nabla\theta\rangle\,, \tag{3.23}$$

$$D_1 = \left\|\nabla^2\theta\right\|^2 + \left\|\nabla^2 \mathbf{q}\right\|^2, \tag{3.24}$$

$$N_1 = Pr\left\langle \mathbf{q}\cdot\nabla\theta\nabla^2\theta\right\rangle + \left\langle \mathbf{q}\cdot\nabla\mathbf{q}\cdot\nabla^2\mathbf{q}\right\rangle. \tag{3.25}$$

Now, we recall the embedding theorem and some results as

$$\|\nabla w\| \leq \|\nabla \mathbf{q}\|\,,\ \sup|G| \leq C^*\left\|\nabla^2 G\right\|\,,\ G \in \{\mathbf{q},\theta\}\,. \tag{3.26}$$

Here, the value of C^* has been given by Galdi and Straughan [6], which represents the computable positive constant depending on V.

Therefore, from Eq. (3.23) using (3.16), (3.24), and (3.26), the Cauchy-Schwarz and the Young's inequalities, we get

$$b_o I_1 = b_0\pi^2\left\langle \nabla w\frac{(2G-1)\,R^{1/2}}{G\pi^2}\nabla\theta\right\rangle \leq \frac{b_o\varepsilon_o^2}{2}D_1 + \frac{(2G-1)^2\,b_o R}{2G^2\varepsilon_o^2\pi^4}D_0,$$

defining

$$D_2 = \frac{a_o}{2}D_0 + \frac{b_o}{2}D_1, \tag{3.27}$$

and choosing

$$\varepsilon_o^2 = 1 \text{ and } b_o = \frac{a_o G^2\pi^4}{(2G-1)^2\,R}.$$

It then easily follows that

$$b_o I_1 \leq D_2. \tag{3.28}$$

Now, estimate N_1 and N_0 by using (3.20), (3.21), (3.24), (3.26), and (3.27), we find the results as

$$N_1 \leq C^* \left(\frac{2}{b_0}\right)^{3/2} \left\{ (Pr)^{1/2} + \left[1 + \frac{FL}{n+L}\right]^{-1/2} \right\} D_2 E_g^{1/2}, \tag{3.29}$$

$$N_0 \leq C^* \left(\frac{2}{b_0}\right)^{3/2} \left\{ (Pr)^{1/2} + 2\lambda_1 + 2\left(\frac{b_0\lambda_2}{a_0}\right)^{1/2} \right\} D_2 E_g^{1/2}. \tag{3.30}$$

Using Eqs. (3.27)–(3.30) in Eq. (3.22), we get

$$\frac{dE_g(t)}{dt} \leq -D_2 \left(1 - \tilde{A} E_g^{1/2}\right), \tag{3.31}$$

where

$$\tilde{A} = C^* \left(\frac{2}{b_o}\right)^{3/2} \left\{ b_o \left[(Pr)^{1/2} + \left(1 + \frac{FL}{n+L}\right)^{-1/2} \right] + (Pr)^{1/2} + 2\lambda_1 + 2\left(\frac{b_o\lambda_2}{a_o}\right)^{1/2} \right\}. \tag{3.32}$$

This estimation allows us to show a theorem for conditional nonlinear stability.

Theorem 3.1. *There exists a constant $K^* > 0$, such that the inequality*

$$E_g(t) \leq E_g(0) \exp\left\{ \left(1 - \tilde{A} E_g^{1/2}(0)\right) (-K^*)\, t \right\}, \tag{3.33}$$

holds $\forall\ t \geq 0$, if we consider $0 < m < 1$ and $E_g(0) < \tilde{A}^{-2}$, where the value of $\tilde{A}$ is given by Eq. (3.32).

Proof. The given hypothesis together with inequality (3.31) confirms that

$$\frac{dE_g(0)}{dt} < 0.$$

Therefore, by using recursive argument, the result obtained from inequality (3.31) as

$$\frac{dE_g(t)}{dt} \leq -D_2 \left(1 - \tilde{A} E_g^{1/2}(0)\right) \quad \forall\ t \geq 0. \tag{3.34}$$

To show the existence of $K^* > 0$ such that

$$-K^* E_g(t) \geq -D_2. \tag{3.35}$$

From Eq. (3.20), using Poincaré-type inequalities and Eqs. (3.16), (3.24), and (3.27), we have

$$E_g \leq \frac{1}{\pi^2} \left\{ Pr + 2\left(1 + \frac{FL}{n+L}\right) \right\} \left(1 + \frac{m}{1-m}\right) D_2.$$

Let $k_o > 0$, such that

$$k_o \geq \frac{m}{1-m}, \tag{3.36}$$

we have

$$E_g \leq \frac{1}{\pi^2} \left\{ Pr + 2\left(1 + \frac{FL}{n+L}\right) \right\} (1 + k_o)\, D_2.$$

Letting

$$K^* = \frac{\pi^2}{\left\{ Pr + 2\left(1 + \frac{FL}{n+L}\right) \right\} (1 + k_o)},$$

with k_o given by (3.36), then from (3.34) and (3.35), we obtain

$$\frac{dE_g(t)}{dt} \leq -K^* E_g(t) \left[1 - \tilde{A} E_g^{1/2}(0)\right], \quad \forall\, t \geq 0. \tag{3.37}$$

Integrating (3.37), we get

$$E_g(t) \leq E_g(0) \exp\left\{-K^* \left[1 - \tilde{A} E_g^{1/2}(0)\right] t\right\}. \tag{3.38}$$

□

Inequality (3.34) yields sufficient conditions to ensure the decay of generalized energy. From inequality (3.38), it follows that $E_g(t) \to 0$ as $t \to \infty$ monotonically. Since K^* involves the effect of collisional frequency, it shows that the collisional frequency played an important role in energy decay.

3.2. **Variational problem.** Returning to Eq. (3.18) to get the maximum of the problem at $m = 1$ by applying the calculus of variation. After applying the transformations $\hat{w} = \sqrt{\lambda_1} w$ and $\hat{\zeta} = \sqrt{\lambda_2}\zeta$, the corresponding Euler-Lagrange equations (dropping caps) are as follows

$$2\nabla^4 w + \left(\frac{G-1}{G}\right) \frac{R^{1/2}}{\lambda_1^{1/2}} \theta_{zz} + \lambda_1^{1/2}\, R^{1/2}\, \nabla_1^2 \theta - T_A^{1/2} \left(\frac{\lambda_1 + \lambda_2}{\lambda_1^{1/2}\, \lambda_2^{1/2}}\right) \zeta_z = 0, \tag{3.39}$$

$$2\nabla^2 \theta_{zz} + \left(\frac{G-1}{G}\right) \frac{R^{1/2}}{\lambda_1^{1/2}} w_{zz} + \lambda_1^{1/2}\, R^{1/2}\, \nabla_1^2 w = 0, \tag{3.40}$$

$$2\nabla^2 \zeta + T_A^{1/2} \left(\frac{\lambda_1 + \lambda_2}{\lambda_1^{1/2}\, \lambda_2^{1/2}}\right) w_z = 0. \tag{3.41}$$

Now, the plane tiling form is assumed as

$$(w, \zeta, \theta) = [W(z), Z(z), \Theta(z)]\, \Psi(x, y). \tag{3.42}$$

Here,

$$\nabla_1^2 \Psi + a^2 \Psi = 0, \tag{3.43}$$

'a' is the wave number.

We find that Eqs. (3.39)–(3.41), with the help of expressions (3.42) and (3.43) gives

$$2\left(D^2 - a^2\right)^2 W + R^{1/2} \left(\frac{G-1}{G} \frac{D^2}{{\lambda_1}^{1/2}} - {\lambda_1}^{1/2} a^2\right) \Theta - T_A^{1/2} \left(\frac{\lambda_1 + \lambda_2}{\lambda_1^{1/2}\, \lambda_2^{1/2}}\right) DZ = 0, \tag{3.44}$$

$$2\left(D^2 - a^2\right) D^2 \Theta + \left(\frac{G-1}{G}\right) \frac{R^{1/2}}{\lambda_1^{1/2}} D^2 W - \lambda_1^{1/2}\, R^{1/2}\, a^2 W = 0, \tag{3.45}$$

$$2\left(D^2 - a^2\right) Z + T_A^{1/2} \left(\frac{\lambda_1 + \lambda_2}{\lambda_1^{1/2}\, \lambda_2^{1/2}}\right) DW = 0. \tag{3.46}$$

The BCs appropriate to Eqs. (3.44)–(3.46) are given as:
For free-free boundaries

$$W = 0,\ D^2 W = 0,\ DZ = 0,\ \Theta = 0,\ D^2 \Theta = 0 \text{ at } z = 0,\ 1. \tag{3.47}$$

For rigid-free boundaries

$$\begin{aligned} &W = 0,\ DW = 0,\ Z = 0,\ \Theta = 0,\ D^2 \Theta = 0 \text{ at } z = 0, \\ &W = 0,\ D^2 W = 0,\ DZ = 0,\ \Theta = 0,\ D^2 \Theta = 0 \text{ at } z = 1. \end{aligned} \tag{3.48}$$

For rigid-rigid boundaries

$$W = 0,\ DW = 0,\ Z = 0,\ \Theta = 0,\ D^2 \Theta = 0 \text{ at } z = 0,\ 1. \tag{3.49}$$

The case of two free-bounding surfaces is of little physical interest and is most appropriate for a stellar atmosphere, but it is mathematically important and its properties guide our analysis. Other bounding surfaces are practically important and represent a logical endpoint within the physical world. Rigid-rigid bounding surfaces are often encountered in various engineering applications, such as laboratory plasmas. Moreover, rigid-rigid boundaries can also impose certain boundary conditions on the plasma, such as the no-slip boundary condition, which states that the velocity of plasma at the boundary should be zero.

4. Numerical and computational analyses

For numerical analysis, the Galerkin-type method has been used to solve Eqs. (3.44)–(3.46) with BCs (3.47)–(3.49). Here we define boundary conditions-compliant solutions as

$$W = \sum_{i=1}^{N} A_i W_i, \tag{4.1}$$

$$\Theta = \sum_{i=1}^{N} B_i \Theta_i, \tag{4.2}$$

$$Z = \sum_{i=1}^{N} C_i Z_i, \tag{4.3}$$

in which $W_i,\ \Theta_i,\ Z_i$ are base functions satisfying the BCs and $A_i,\ B_i,\ C_i$ are unknown coefficients, $i = 1, 2, 3, ..., N$. Accordingly, W, Θ and Z are taken for different boundaries.

For free-free bounding surfaces, the BCs are given by (3.47), the exact solutions [5] are

$$W_i = \sin(i\pi z),\ \Theta_i = \sin(i\pi z) \text{ and } Z_i = \left(\frac{2\Omega d}{\nu}\right)\left(\frac{i\pi}{i^2\pi^2 + a^2}\right)\cos(i\pi z). \tag{4.4}$$

For rigid-free bounding surfaces, the BCs are given by (3.48), the basis functions [19] are as

$$W_i = z^2\,(1-z)\left[(i+2) - 2z^i\right],\ \Theta_i = z^i - 2z^{i+2} + z^{i+3} \text{ and } Z_i = 3z^{i+1} - 2z^{i+2}. \tag{4.5}$$

For rigid-rigid bounding surfaces, the BCs are given by (3.49), the basis functions [19] are as

$$W_i = z^{i+1} - 2z^{i+2} + z^{i+3},\ \Theta_i = z^i - 2z^{i+2} + z^{i+3} \text{ and } Z_i = 3z^{i+1} - 2z^{i+2}. \tag{4.6}$$

When the Eqs. (4.1)–(4.3) are substituted into Eqs. (3.44)–(3.46), and apply the Galerkin procedure, a linear system of homogeneous equations is obtained

$$J_{ji}A_i + H_{ji}B_i + K_{ji}C_i = 0, \tag{4.7}$$

$$M_{ji}A_i + N_{ji}B_i + O_{ji}C_i = 0, \tag{4.8}$$

$$V_{ji}A_i + Q_{ji}B_i + S_{ji}C_i = 0. \tag{4.9}$$

In order to have a non-trivial solution of Eqs. (4.7)–(4.9),

$$\begin{vmatrix} J_{ji} & H_{ji} & K_{ji} \\ M_{ji} & N_{ji} & O_{ji} \\ V_{ji} & Q_{ji} & S_{ji} \end{vmatrix} = 0. \tag{4.10}$$

From Eq. (4.10), with the help of Mathematica software, we get Rayleigh number 'R' in terms of wave number, Taylor number and coupling parameters. The conditions $\frac{dR}{d\lambda_1} = 0$ and $\frac{dR}{d\lambda_2} = 0$ gives the optimal values of λ_1 and λ_2. The optimal values of λ_1 and λ_2 for different boundary conditions are found as, $\lambda_1 = \lambda_2 = \frac{\pi^2}{a^2}\frac{G-1}{G}$ (for free-free boundary conditions), $\lambda_1 = \lambda_2 = \frac{936(G-1)}{95a^2G}$ (for rigid-free boundary conditions) and $\lambda_1 = \lambda_2 = \frac{108(G-1)}{11a^2G}$ (for rigid-rigid boundary conditions).

The Rayleigh number for the optimal values of λ_1 and λ_2 are found as follows:
For free-free boundaries

$$R = \frac{G(a^6 + 3a^4\pi^2 + 3a^2\pi^4 + \pi^6 + \pi^2 T_A)}{a^2(G-1)}. \tag{4.11}$$

For rigid-free boundaries

$$R = \frac{2G(168 + 17a^2)(381024 + 154224a^2 + 12828a^4 + 494a^6 + 1521T_A)}{1235a^2(42 + 13a^2)(G-1)}. \tag{4.12}$$

For rigid-rigid boundaries

$$R = \frac{G(168 + 17a^2)(42336 + 15120a^2 + 708a^4 + 26a^6 + 81T_A)}{33a^2(42 + 13a^2)(G-1)}. \tag{4.13}$$

5. Instability analysis (linear)

By ignoring the nonlinear terms in Eqs. (3.1)–(3.4), we get the linearized form of non-dimensional equations

$$\nabla \cdot \mathbf{q} = 0, \tag{5.1}$$

$$\frac{\partial \mathbf{q}}{\partial t} = -\nabla p + R^{1/2}\theta\hat{\mathbf{k}} + \nabla^2\mathbf{q} + FL\left(\mathbf{q}_d - \mathbf{q}\right) + T_A^{1/2}\left(\mathbf{q} \times \hat{\mathbf{k}}\right), \tag{5.2}$$

$$Pr\frac{\partial \theta}{\partial t} = \nabla^2\theta + \left(1 - \frac{1}{G}\right)R^{1/2}w, \tag{5.3}$$

$$\frac{\partial \mathbf{q}_d}{\partial t} = -L\left(\mathbf{q}_d - \mathbf{q}\right). \tag{5.4}$$

5.1. Analysis into normal modes.

Using Eq. (3.5), Eq. (5.2) becomes

$$\left[1 + FL(n+L)^{-1}\right]n\mathbf{q} = -\nabla p + R^{1/2}\theta\hat{\mathbf{k}} + \nabla^2\mathbf{q} + T_A^{1/2}\left(\mathbf{q} \times \hat{\mathbf{k}}\right). \tag{5.5}$$

Now, applying the operator $\hat{\mathbf{k}} \cdot$ curl and $\hat{\mathbf{k}} \cdot$ curl curl on Eq. (5.5), we have

$$\left[1 + FL(n+L)^{-1}\right]n\zeta = \nabla^2\zeta + T_A^{1/2}w_z, \tag{5.6}$$

$$\left[1 + FL(n+L)^{-1}\right]n\nabla^2 w = R^{1/2}\nabla_1^2\theta + \nabla^4 w - T_A^{1/2}\zeta_z, \tag{5.7}$$

where w and ζ are the $z-$components of the velocity and vorticity.

Also, from Eq. (5.3), we get

$$Pr\frac{\partial \theta_z}{\partial t} = \nabla^2\theta_z + \left(1 - \frac{1}{G}\right)R^{1/2}w_z. \tag{5.8}$$

Now, we assume w, θ and ζ in the form

$$(w, \theta, \zeta) = \left[W(z), \Theta(z), Z(z)\right]\exp\left\{\iota\left(k_x x + k_y y\right) + nt\right\}. \tag{5.9}$$

Now, by using (5.9), the Eqs. (5.6)–(5.8) become

$$n\left(1 + \frac{FL}{n+L}\right)Z = \left(D^2 - a^2\right)Z + T_A^{1/2}DW, \tag{5.10}$$

$$n\left(1 + \frac{FL}{n+L}\right)\left(D^2 - a^2\right)W = \left(D^2 - a^2\right)^2 W - R^{1/2}a^2\Theta - T_A^{1/2}DZ, \tag{5.11}$$

$$nPr(D^2\Theta) = \left(D^2 - a^2\right)D^2\Theta + \left(\frac{G-1}{G}\right)R^{1/2}D^2 W. \tag{5.12}$$

The associated BCs are the same as (3.47)–(3.49).

5.2. **Numerical and computational analyses.** For solving Eqs. (5.10)–(5.12) with BCs (3.47)–(3.49), we use the same procedure as mentioned in section 4.

For neutral stability, the real part of n should vanish. So, we choose $n = \iota\omega$, where ω is the non-dimensional frequency of the harmonic disturbances. Therefore, the value of R is of the form

$$R = R_r + \iota\omega R_i, \tag{5.13}$$

where R_r is the real part of the Rayleigh number and R_i is the imaginary part. Since the Rayleigh number is a physical quantity, it can't have imaginary values [2]. Hence, from Eq. (5.13), we have two cases either $\omega = 0$ or $\omega \neq 0$ and $R_i = 0$.

5.2.1. *Stationary mode of convection.* The case of $\omega = 0$ corresponds to the stationary convection mode. In this case, the Rayleigh number ($R = R_r$) for different bounding surfaces is the same as mentioned in Eqs. (4.11)–(4.13). Here, the same values of the Rayleigh number confirm the non-existence of sub-critical regions and it leads to a strong result for global stability [15]. Also, the Rayleigh number for stationary convection mode is represented by R_{stat}.

5.2.2. *Oscillatory mode of convection.* The case of $\omega \neq 0$ implies that R_i must vanish. This case corresponds to the oscillatory mode of convection. From the condition $R_i = 0$, we get an algebraic equation in terms of ω^2. After solving this equation, we get the value of ω^2. Here, the values of ω^2 must be positive, otherwise, there will be no oscillatory mode of convection [7]. Using the values of ω^2 in R_r, we get the value of oscillatory Rayleigh number (R_{osc}).

6. Results and discussion

The preceding analysis demonstrates that the value of 'R' for both nonlinear and linear (stationary convection) analyses is the same. Consequently, a sub-critical region is not possible and it leads to a strong result for global stability. For free-free bounding surfaces, an exact solution is used to obtain 'R', whereas for rigid-free and rigid-rigid bounding surfaces, approximate solutions are used. The Galerkin method has been employed to computationally determine 'R'. The results indicate that the collisional effect plays a role in energy decay and it also contributes to R_{osc}, whereas it doesn't affect the value of the R_{stat}. It is worth noting that for free-free bounding surfaces (excluding the effect of compressibility from present work), the Rayleigh number is the same as presented in the study by Sharma and Sharma [10] in the absence of a magnetic field, this validates the finding of our preset work.

Figure 2 shows the variation of Rayleigh numbers for oscillatory and stationary modes of convection with wave number (a) for free-free boundaries. It is depicted from Figure 2(a) that as we increase the Taylor number (T_A) the value of R_{stat} also increases, which concludes that T_A delays the onset of convection. Also, it has been found that for $T_A = 1000$ the range of a for which oscillatory mode appears is $0 < a < 1.63542$, for $T_A = 5000$ it is found to be $0 < a < 3.40304$, and for $T_A = 10000$ the range is $0 < a < 4.14199$. This concludes that with the increase of T_A, the region of wave number (a) for oscillatory convection also increases. From Figure 2(b) it has been clear that the collisional frequency parameter (L) affects the values of R_{osc}. Now, as the Eq. (4.11) doesn't involve L, the value of R_{stat} remains unaffected by the variation of L, which can be observed from Figure 2(b). Also, Figure 2(b) deduces that the value of R_{osc} is decreasing with the increase of the L. Here, the oscillatory mode of convection appears for $0 < a < 1.63542$, and this range of wave number remains the same for $L = 0.5, 1.0, 1.5$.

Figure 3 illustrates the variation of Rayleigh number for stationary and oscillatory modes of convection with wave number for rigid-free boundaries. It can be seen from Figure 3(a) that with the increase of the T_A the value of R_{stat} also increases, which suggests that the T_A enhances the stability of the system for stationary convection. Also, the range of wave number (a) for the oscillatory mode of convection is $0 < a < 2.13084$ for $T_A = 1000$, $0 < a < 3.31002$ for $T_A = 5000$ and $0 < a < 3.86358$ for $T_A = 10000$. From this, we can conclude that the range of wave number (a) increases for the oscillatory mode of convection, with an increased T_A. From Figure 3(b), it has been clear that the R_{osc} has been influenced by the variation of the collisional frequency parameter (L). Also, it has been depicted from the figure that R_{osc} is increasing with the increase of L. The range of wave number (a), for which the oscillatory pattern prevails is found to be $0 < a < 2.13084$. As Eq. (4.12) doesn't involve the collisional frequency parameter (L), hence R_{stat} remains unaffected by the variation of L.

Figure 4 represents the variation of Rayleigh number for oscillatory and stationary modes of convection with wave number (a) for rigid-rigid boundaries. Figure 4(a) makes it abundantly evident that when T_A increases, the value of

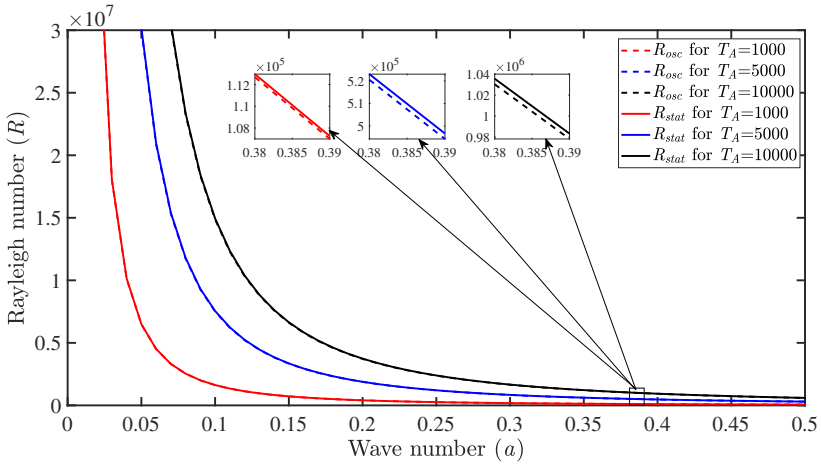

(a)

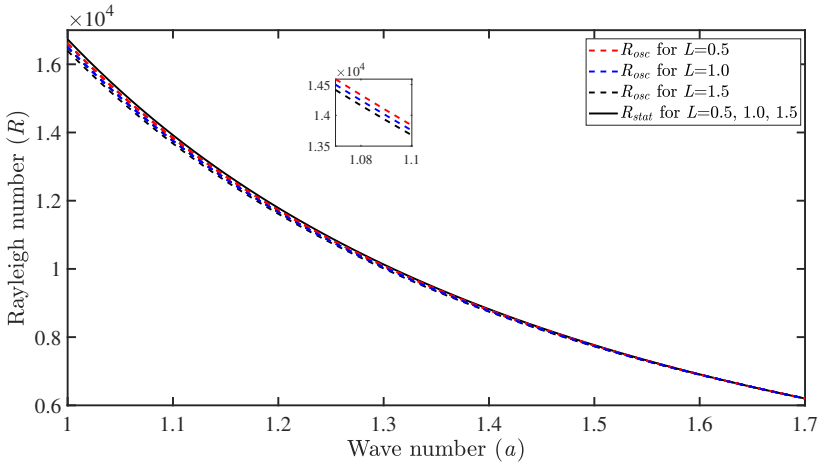

(b)

FIGURE 2. Variation of Rayleigh number with wave number for different values of (a) T_A, and (b) L, for free-free boundaries at $G = 3$, $Pr = 1$ and $F = 0.5$.

the R_{stat} also increases, which concludes that the T_A improves the stability of the system for stationary convection. Additionally, it has found that the range of wave number (a) for the oscillatory mode of convection is $0 < a < 1.8761$ for $T_A = 1000$, $0 < a < 3.14923$ for $T_A = 5000$ and $0 < a < 3.73435$ for $T_A = 10000$. This leads us to the conclusion that when T_A increases, the range of wave number (a) expands for the oscillatory mode of convection. The influence of variation of L on R_{osc} has been evident from Figure 4(b). Also, it has been depicted from the figure that R_{osc} is increasing with the increase of L. The oscillatory convection appears for $0 < a < 1.8761$. Since the collisional frequency parameter (L) is not included in Eq. (4.13), the stationary convection is unaffected by the variation of L.

Figure 5 illustrates the theoretical relationship between the Taylor number T_A and the critical Rayleigh number R_c for the stationary mode of convection across three different combinations of bounding surfaces. It is evident that as T_A increases, the value of R_c also increases for all combinations of bounding surfaces. This trend indicates that rotation has a stabilizing effect on convection. The rotational forces reduce the velocity of the partially-ionized plasma in the boundary layer, limiting the rate of heat transfer from the lower to the upper layer. Additionally, rotation aids

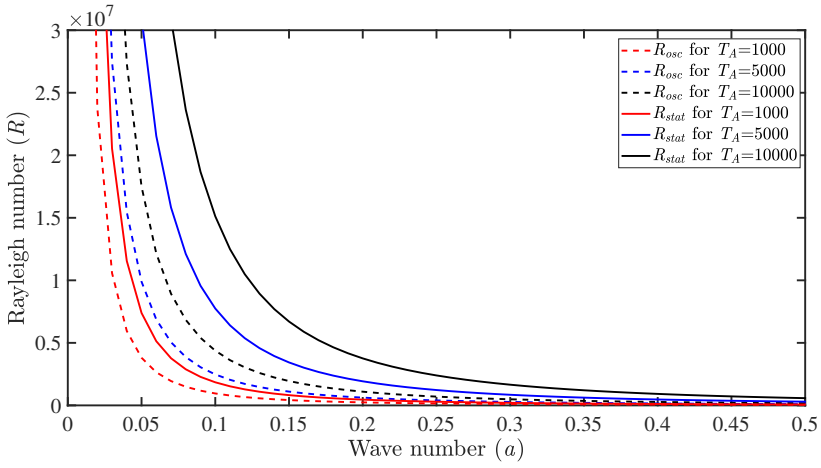

(a)

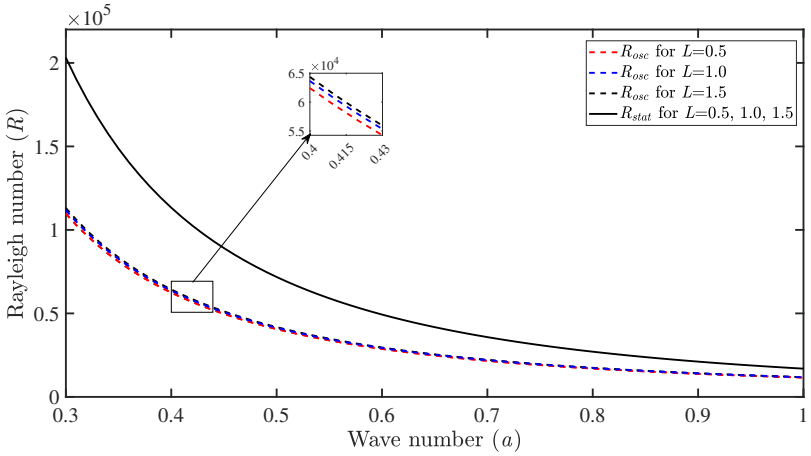

(b)

FIGURE 3. Variation of Rayleigh number with wave number for different values of (a) T_A, and (b) L, for rigid-free boundaries at $G = 3$, $Pr = 1$ and $F = 0.5$.

in the formation and stability of well-defined convective cells, leading to stronger convective motion and, consequently, higher critical Rayleigh numbers.

For low Taylor numbers, free-free bounding surfaces exhibit greater susceptibility to deformation and temperature fluctuations, which can destabilize the formation of convective cells. This results in weaker convective motion and lower Rayleigh numbers. However, at high Taylor numbers, these fluctuations instead promote the stability of the convective motion by enhancing the formation and interaction of convective cells. This enhances the mixing efficiency of the plasma and increases the heat transfer rate, leading to a higher R_c.

In contrast, rigid-rigid bounding surfaces offer more stable temperature conditions at low Taylor numbers, which fosters the development and stability of well-defined convective cells. As a result, the convective motion is stronger, and the critical Rayleigh number is higher compared to free-free bounding surfaces. However, at high Taylor numbers, the rigidity of the boundary suppresses interaction between the larger convective cells that form. The reduced interaction

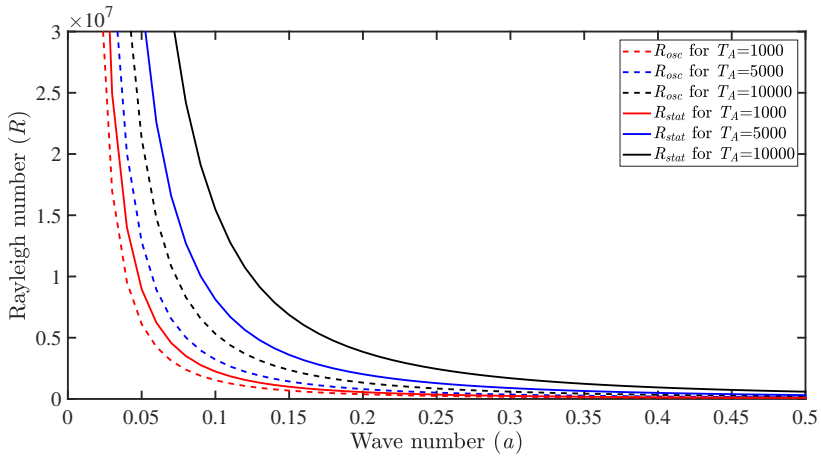

(a)

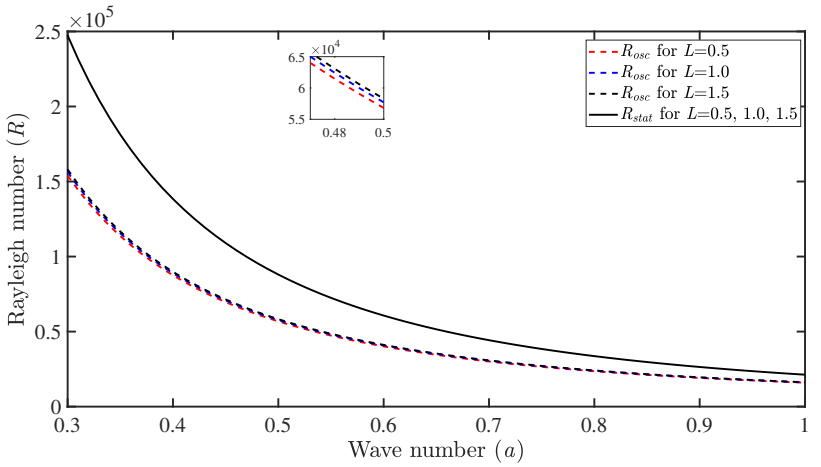

(b)

FIGURE 4. Variation of Rayleigh number with wave number for different values of (a) T_A, and (b) L, for rigid-rigid boundaries at $G = 3$, $Pr = 1$ and $F = 0.5$.

results in less efficient mixing and a lower heat transfer rate, causing the Rayleigh number to be lower compared to that of free-free surfaces.

Thus, rotation stabilizes the system in all cases, and the impact of bounding surfaces becomes more pronounced at high Taylor numbers, with free-free surfaces eventually surpassing rigid-rigid surfaces in terms of convective efficiency and higher critical Rayleigh numbers.

It has been found that compressibility delays the onset of thermal convection by increasing the Rayleigh number, meaning that convection occurs later in compressible partially-ionized plasma compared to incompressible plasma. This effect is especially notable when the compressibility parameter G exceeds 1, as discussed by Sharma and Sunil [12]. However, for the presence of compressibility in the current study, the cases $G = 1$ and $G < 1$ are not pertinent, as they lead to infinite and negative Rayleigh numbers, which are irrelevant to the objective of the present work. From Figure 6, it is evident that for compressible partially-ionized plasma, as the values of the compressibility parameter increase, the values of R_c decrease, implying that compressibility hastens the onset of convection. Also, it has been

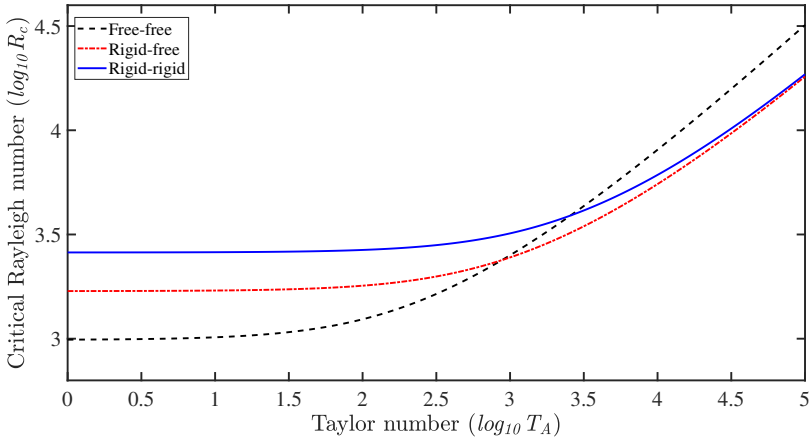

FIGURE 5. Variation of critical Rayleigh number (R_c) with Taylor number (T_A) for a fixed value of $G = 3$ for the distinct combination of bounding surfaces for the stationary mode of convection.

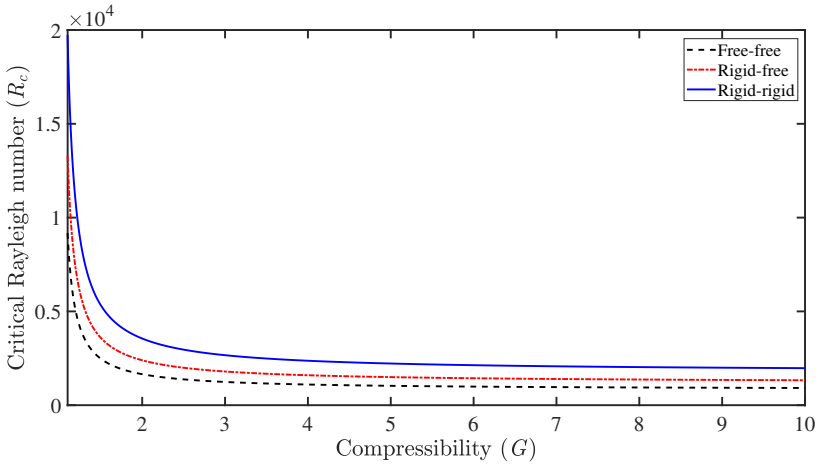

FIGURE 6. Variation of critical Rayleigh number (R_c) with compressibility parameter (G) for a fixed value of $T_A = 100$ for the distinct combination of bounding surfaces for the stationary mode of convection.

observed that for very high compressibility values, the plasma behaves almost incompressibly. The analysis confirms that the rigid-rigid bounding surfaces offer the greatest thermal stability for confining partially-ionized plasma.

To further validate our numerical results against the analytical findings, we analyzed the derivatives of the Rayleigh number with respect to key parameters. For rotation, we found that $dR/dT_A > 0$, indicating the stabilizing effect of rotation on the system. Conversely, for compressibility, $dR/dG < 0$, which points to the destabilizing influence of compressibility. These analytical observations align well with the numerical results, further reinforcing the reliability and consistency of our study's findings.

This study provides crucial insights into the stability of rotating, partially-ionized plasmas, which are relevant to both theoretical and applied fields. The results are significant for understanding the behaviour of such plasmas in astrophysical systems (e.g., stellar atmospheres and magnetospheres) where rotation and collisional effects influence convection and energy dissipation. In fusion energy research, the findings contribute to optimizing plasma stability

in devices like tokamaks, where maintaining stability is key for sustained nuclear fusion reactions. Also, the study has industrial applications in plasma-assisted processes, where controlling plasma stability can enhance efficiency and performance. From a theoretical standpoint, our approach to global stability in partially-ionized plasma systems also extends to broader dynamical systems, offering valuable insights into stability in other fluid and complex systems.

7. Conclusions

This study investigated the thermal convection of a rotating, compressible, partially-ionized plasma layer heated from below, considering three distinct bounding surface configurations. The motivation behind this research lies in the crucial role that rotation plays in influencing thermal convection in partially-ionized plasma, which has important applications across multiple fields. The key conclusions from this study are summarized as follows:

- Stationary convection in partially-ionized plasma exhibits identical instability and stability boundaries for all three types of bounding surfaces, confirming global stability.
- The collisional effects disappear for stationary convection, and therefore do not influence system stability for stationary convection. However, collisional frequency plays a significant role in energy dissipation, as demonstrated in our theorem.
- Rotation reduces the velocity of partially-ionized plasma within the boundary layer, leading to a decrease in heat transfer from the bottom to the top of the layer. This reduction in heat transfer delays the onset of convection, thereby enhancing the stability of the system.
- For low rotation rates, the plasma confined between rigid-rigid bounding surfaces is the most stable, whereas plasma confined between free-free surfaces is the least stable.
- At higher rotation rates, the stability pattern reverses, with free-free bounding surfaces providing the most stability and rigid-rigid surfaces the least.
- Oscillatory modes of convection are introduced by rotational effects and influenced by both collisional frequency and rotation.
- Compressibility delays the onset of thermal convection by increasing the Rayleigh number in partially-ionized plasma. However, as the compressibility parameter increases, the critical Rayleigh number decreases, hastening the onset of convection.

These findings offer significant insights into the dynamics of partially-ionized plasmas across different boundary conditions. For instance, the stabilization provided by rigid-rigid surfaces at low rotation rates, and by free-free surfaces at higher rates, can be instrumental in optimizing plasma confinement in engineering applications such as tokamaks. Moreover, understanding the role of collisional effects in energy dissipation is critical for addressing energy loss mechanisms in astrophysical settings, such as solar wind propagation, as well as in industrial plasma technologies. The impact of compressibility in delaying convection provides further predictive capabilities, aiding in the management and control of such plasma systems under varying conditions.

Future research directions could include investigating the influence of surface tension on thermal convection in partially-ionized plasma through both linear and nonlinear analyses across different bounding surfaces. Additionally, exploring the effects of varying ionization levels, Hall currents, and finite Larmor radius on stability and convection thresholds would greatly expand the scope of the study. The application of machine learning techniques to control Rayleigh-Bénard convection in partially-ionized plasma also presents a promising avenue for advanced control and optimization strategies.

Acknowledgments

The authors sincerely thank the esteemed editorial board and reviewers for their invaluable comments and insightful suggestions, which have significantly enhanced the quality and depth of this work.

References

[1] H. Alfvén, *On the origin of the solar system*, Clarendon Press, Oxford, 1954.
[2] R. Chand, D. Yadav, K. Bhattacharyya, and M. K. Awasthi, *Thermal convection in a layer of micropolar nanofluid*, Asia-Pac. J. Chem. Eng., *16* (2021), e2681.

[3] V. Chandel and Sunil, *Influence of magnetic fields and bounding surface configurations on thermal convection in partially ionised plasmas: nonlinear and linear stability analyses*, Pramana - J. Phys., *98* (2024), 107.
[4] V. Chandel, Sunil, and P. Sharma, *Study of global stability of rotating partially-ionized plasma saturating a porous medium*, Spec. Top. Rev. Porous Media: Int. J., *15* (2024), 27–46.
[5] S. Chandrasekhar, *Hydrodynamic and hydromagnetic stability*, Dover, New York, 1981.
[6] G. P. Galdi and B. Straughan, *A nonlinear analysis of the stabilizing effect of rotation in the Bénard problem*, Proc. R. Soc. Lond. A, *402* (1985), 257–283.
[7] A. Garg, Y. D. Sharma, and S. K. Jain, *Onset of triply diffusive thermo-bio-convection in the presence of gyrotactic microorganisms and internal heating into an anisotropic porous medium: Oscillatory convection*, Chin. J. Phys., *84* (2023), 173-188.
[8] V. Krishan, *Different representations of a partially ionized plasma*, J. Astrophys. Astr., *43* (2022), 43.
[9] R. K. Pensia, V. Shrivastava, and A. K. Patidar, *Magneto-thermal instability of rotating partially ionized Hall plasma flowing through porous medium*, PSIJ, *8* (2015), PSIJ.10134.
[10] R. C. Sharma and K. C. Sharma, *Thermal instability of a partially ionized plasma*, Aust. J. Phys., *31* (1978), 181–187.
[11] R. C. Sharma and Sunil, *Thermal instability of a compressible finite Larmor radius, Hall plasma in porous medium*, Phys. Plasmas, *2* (1995), 1886–1892.
[12] Y. D. Sharma and Sunil, *Compressibility and Hall effects on thermosolutal instability of a partially ionized plasma in porous medium*, Polym. Plast. Technol. Eng., *35* (1996), 169–186.
[13] R. Soler and J. L. Ballester, *Theory of fluid instabilities in partially ionized plasmas: An overview*, Front. Astron. Space Sci., *9* (2022), 789083.
[14] E. A. Spiegel and G. Veronis, *On the Boussinesq approximation for a compressible fluid*, Astrophys. J., *131* (1960), 442–447.
[15] B. Straughan, *The energy method, stability, and nonlinear convection*, Springer-Verlag, New York, 2004.
[16] Sunil, S. Choudhary, and A. Mahajan, *Conditional stability for thermal convection in a rotating couple-stress fluid saturating a porous medium with temperature and pressure dependent viscosity*, J. Geophys. Eng., *10* (2013), 045013.
[17] Sunil and A. Mahajan, *A nonlinear stability analysis for magnetized ferrofluid heated from below*, Proc. R. Soc. A, *464* (2008), 83–98.
[18] Sunil and Y.D. Sharma, *Rayleigh-Taylor instability of a partially ionized rotating plasma in the presence of a variable horizontal magnetic field in porous medium*, Polym. Plast. Technol. Eng., *35* (1996), 221–231.
[19] D. Yadav, R. Bhargava, and G. S. Agrawal, *Thermal instability in a nanofluid layer with a vertical magnetic field*, J. Eng. Math., *80* (2013), 147–164.